Similarity of the coupled equations for RF waves in a tokamak

Cite as: Phys. Plasmas **26**, 012505 (2019); https://doi.org/10.1063/1.5066288
Submitted: 13 October 2018 • Accepted: 18 December 2018 • Published Online: 09 January 2019

Jungpyo Lee, David Smithe, Erwin F. Jaeger, et al.

Physics of Plasmas ARTICLE scitation.org/journal/php

Similarity of the coupled equations for RF waves in a tokamak

Cite as: Phys. Plasmas **26**, 012505 (2019); doi: 10.1063/1.5066288
Submitted: 13 October 2018 · Accepted: 18 December 2018 · Published Online: 09 January 2019

Jungpyo Lee,[1,2] David Smithe,[3] Erwin F. Jaeger,[4] Robert W. Harvey,[5] and Paul T. Bonoli[2]

AFFILIATIONS

[1] Hanyang University, Nuclear Engineering Department, Seoul 04763, South Korea
[2] MIT, Plasma Science and Fusion Center, Cambridge, Massachusetts 02139, USA
[3] Tech-X, Boulder, Colorado 80303, USA
[4] XCEL Engineering, Oak Ridge, Tennessee 37830, USA
[5] CompX, Del Mar, California 92014, USA

ABSTRACT

In this paper, a similarity relation between RF wave systems in tokamaks is found theoretically by investigating scaling conditions of plasma density and temperature, tokamak size and background magnetic fields, and RF wave frequency and power. The scaling conditions simultaneously satisfy Maxwell's equations, the Grad-Shafranov equation, and the Fokker-Planck equation. The consistency of the scaling with transport equations is examined by several empirical and theoretical scalings for confinement time. The similarity found in this paper is useful to investigate the possibility of the test system for RF wave experiments and verify the coupled numerical codes for the wave modeling.

I. INTRODUCTION

Finding a scaling law in a system is a commonly sought objective in many experiments and simulations (e.g., tokamak confinement time scalings[1–3]) because it can be used to design and optimize the system. There are additional benefits of finding an analytical similarity based on the scaling law, which are listed below. First, if it is practically difficult to represent the system in experiments because it is too large, expensive, or hazardous, using the similarity enables alternative experiments that are smaller, less expensive, or less hazardous. For example, a wind tunnel is a reduced test system to model a large fluid dynamic system using the scaling law with some dimensionless variables (e.g., Reynolds number),[4] and some laboratory experiments are used to model MHD phenomena in astrophysics.[5] Second, the dimension of partial differential equations can be reduced by introducing similarity variables, which reduce the computational cost significantly to solve the problem.[6] Finally, the analytical similarity can be used to verify numerical codes. Specifically, if some numerical codes are coupled to find a set of self-consistent solutions, finding whether the solutions follow the scaling relations is an efficient way to verify the coupling. The fact that the numerical solutions satisfy the similarity is not a sufficient condition but is a necessary condition of the code verification. The similarity must hold regardless of the degree of nonlinearity in the coupling.

In this paper, we find a similarity relation of RF waves in plasmas, which are used for heating and current drive in a tokamak. There are several experimental and theoretical studies based on the similarity of the RF waves in different tokamaks. For example, when designing the ICRF (ion cyclotron range of frequency) wave heating scenarios on ITER,[7] many experiments on the existing tokamaks have been examined by setting the similar wave conditions.[8–10] One can expect the similar phenomena in ITER as observed in JET experiments, which have proven the important ICRF physics such as the optimized minority ion concentration, mode conversion to slow waves, and finite Larmor radius effects in different plasmas: (^{3}*He*)H, (T)H, or (H)D. Additionally, the ITER antenna design and coupling problems are investigated in JET based on the similarity of the system.[10–12] These similarities are obtained by matching some important key parameters (e.g., the cyclotron frequency, species, and antenna size), but it cannot guarantee the exact equivalent physical effects between two different systems because of other non-matched parameters, as considered in this paper. Although many engineering constraints (e.g., magnetic fields and

machine size) likely reduce the chance of the rigorous similarity of all parameters, we analyze the possibilities theoretically.

The rigorous similarity of the RF wave system in a tokamak is found in this paper by investigating the coupled equations: Maxwell's equations, Grad-Shafranov equation, transport equation, and Fokker-Planck equation. It is well known that Maxwell's equations for the electromagnetic wave propagation and damping in plasmas have a similarity with some dimensionless parameters using wave frequency ω, plasma frequency $\omega_p = n_s e^2 Z_s^2/\epsilon_0 m_s$, cyclotron frequency $\omega_c = Z_s e B_0/m_s$, and the normalized length scale.[13] Here, n_s, m_s, and Z_s are the density, mass, and charge of the species s, respectively, e is the electron charge, ϵ_0 is the vacuum dielectric constant, and B_0 is the background magnetic field intensity. However, it is not clear whether there is a universal similarity of the RF system when Maxwell's equation is coupled with other equations for the tokamak system. For example, the Grad-Shafranov equation is solved for the background magnetic field,[14] the transport equation is solved for the plasma density and temperature profiles,[1–3] and the Fokker-Planck equation is solved to include the kinetic effects due to non-Maxwellian distribution functions.[15–17]

In principle, there is no reason that there exists a common scaling between the equations because each equation is derived in the different time and length scales with different assumptions. Maxwell's equations in plasmas describe Faraday's law and Ampère's law for the high wave frequency by including the momentum equation for the perturbed plasma particles due to the waves. On the other hand, the Grad-Shafranov equation is Ampère's law with the momentum equation by $\mathbf{J}\times\mathbf{B} = \nabla p$, where $\mathbf{J}$ is the static current in the lowest order that is not related to the perturbation by RF waves and p is the static plasma pressure. The Fokker-Planck equation is for the evolution of the distribution function in the slow collisional time scale compared to the RF waves.

By finding the similarity, we examine the possibility of the reduced test system (wind tunnel) for the RF wave system and verify the numerical codes, which are widely used in the RF wave research community. A high power RF system in a large tokamak for heating (e.g., ECH and ICRH systems in ITER[7]) is extremely expensive and takes a high portion of total construction cost.[18] The cost of the RF system is expected to increase significantly for an advanced tokamak in the future because it requires a larger RF power for non-inductive current drive in a steady state operation.[19] Therefore, testing the RF system in a smaller size system with a reduced cost will be significantly beneficial, if it is available. The verification of the numerical codes for the RF system using the similarity can be another important contribution of this study.

The rest of this paper is organized as follows. In Sec. II, we explain how the similarity relation is obtained between the coupled equations by varying the plasma density and temperature, the machine size and magnetic fields, and RF wave frequency and power. In Sec. III, the similarity is used to verify the coupled numerical codes (TORIC[20]-ECOM[21] and AORSA[23]-ECOM[21]-CQL3D[15]). In Sec. IV, the consistency of the scaling with the transport scaling is examined by Goldston empirical scaling,[2] GryoBohm theoretical scaling,[24,25] and ITER design scaling.[3] Finally, in Sec. V, we make a conclusion with a discussion of conditions to violate the similarity.

II. SIMILARITY IN THE COUPLED EQUATIONS

In this section, we find the possible similarity relation by adding the conditions that satisfy the different set of equations. The scaling relations in Sec. II A are obtained to satisfy Maxwell's equations. In Sec. II B, the conditions found in Sec. II A are examined to satisfy both Maxwell's equations and the Grad-Shafranov equation. Finally, in Sec. II C, the other conditions are added to satisfy all three equations: Maxwell's equations, the Grad-Shafranov equation, and the bounce-averaged Fokker-Planck equation.

A. Maxwell's equations

Maxwell's equations for the electromagnetic waves in plasmas[13] can be reduced to

$$\hat{\nabla}\times\hat{\nabla}\times\mathbf{E} = \frac{\omega^2 a^2}{c^2}\left(\mathbf{E} + \frac{\mu i}{\omega}\mathbf{J}_p\right) = \frac{\omega^2 a^2}{c^2}\epsilon\cdot\mathbf{E}, \tag{1}$$

where $\hat{\nabla} = a\nabla$ is the normalized differential operator using the minor radius a and $\mathbf{J}_p$ is the plasma current. Here, the plasma current is modeled by the dielectric tensor

$$\epsilon = \epsilon\left(\frac{\omega_p}{\omega}, \frac{\omega_c}{\omega}, \frac{\mathbf{k}c}{\omega}, \frac{k_\parallel v_t}{\omega}, k_\perp\rho_i\right), \tag{2}$$

where several dimensionless parameters represent the effects of physical quantities on the dielectric tensor; ω_p/ω represents the plasma density n, ω_c/ω represents the background magnetic field B_0, $\mathbf{k}c/\omega$ represents the wave refractive index, $k_\parallel v_t/\omega$ represents the Doppler effect at the plasma temperature T, and $k_\perp\rho$ represents the finite Larmor radius effect.[13] Here, $\mathbf{k}$ is the wave vector that is determined by antenna boundary conditions and dispersion relations in plasmas. Thus, its components parallel and perpendicular to the background magnetic fields, $k_\parallel$ and $k_\perp$, have the dimension of $1/a_{ant}$, if the dispersion is similar. For the rigorous similarity, we assume in this paper that the relative ratios between the antenna length scale a_{ant}, the minor radius a, and the major radius R are the same in the scaling, and so, the major radius can represent all length scales of the tokamak. Additionally, the relative shapes of all geometry in the tokamak (e.g., magnets, vacuum chamber, and antenna location and shape) are assumed to be the same in the scaling.

The scaling relations are obtained in terms of the set of physics variables (m_s, Z_s, n_s, and T_s for the plasmas, B_0 and R for the machine, and ω for the RF waves) to make the dimensionless parameters $\omega_p/\omega, \omega_c/\omega, \mathbf{k}c/\omega, k_\parallel v_t/\omega, k_\perp\rho$ invariant. The following scalings need to be applied for all species simultaneously for the rigorous similarity, and so, we drop the subscripts s for the species in this manuscript below.

Assume that one can change the wave frequency by a multiplication factor α and the major radius by γ

$$\bar{\omega} = \alpha\omega, \quad \bar{\mathrm{R}} = \gamma \mathrm{R}, \tag{3}$$

where the overline of the variable denotes the change of the variable after the scaling. In a real system, the ion mass and charge could be controllable by selecting different ion species for the scaling, but the electron mass and charge are fixed. Because the rigorous similarity holds only when all species change simultaneously, the species mass and charge are not modified in the scaling of this study. If one assumes that the mass and charge are flexible, the scaling relations can have more degrees of freedom, as explained in the Appendix.

For the same dimensionless variables in the dielectric tensor by the scalings in Eq. (3), it needs to satisfy

$$\overline{\mathrm{B}_0} = \alpha \mathrm{B}_0, \quad \bar{n} = \alpha^2 n, \quad \bar{\mathrm{T}} = \alpha^2\gamma^2 \mathrm{T}. \tag{4}$$

Moreover, to have the same factor $\omega^2 a^2/c^2$ on the right hand side in Eq. (1), it requires the additional condition

$$\gamma = \alpha^{-1}. \tag{5}$$

In this condition, the dielectric tensor does not change

$$\bar{\epsilon}\left(\bar{\omega}, \overline{\mathrm{B}_0}, \bar{n}, \bar{\mathrm{R}}, \bar{\mathrm{T}}\right) = \epsilon(\omega, \mathrm{B}_0, n, \mathrm{R}, \mathrm{T}), \tag{6}$$

and the dispersion relation is exactly equivalent in the scaling. Thus, for the equivalent boundary condition and the antenna current, the electric fields of Maxwell's equation solver have the following scaling:

$$\bar{\hat{\mathbf{E}}}\left(\bar{\omega}, \overline{\mathrm{B}_0}, \bar{n}, \bar{\mathrm{R}}, \bar{\mathrm{T}}\right) = \alpha \hat{\mathbf{E}}(\omega, \mathrm{B}_0, n, \mathrm{R}, \mathrm{T}), \tag{7}$$

where $\hat{\mathbf{E}} = \mathbf{E}/\sqrt{P_{abs}}$ is the normalized electric field by the square root of total RF wave power absorption P_{abs}. Here, the dependency of the total power absorption on α is considered because

$$P_{abs} \simeq \int_{\mathrm{Vol}} d\mathbf{r} Re(\mathbf{E}\cdot\mathbf{J}) = \int_{\mathrm{Vol}} d\mathbf{r} Re\left(\mathbf{E}\cdot\frac{\omega}{\mu i}\epsilon\cdot\mathbf{E}\right), \tag{8}$$

for the volume change ($\mathrm{Vol} \propto \mathrm{R}^3$).

B. Grad-Shafranov equation

The background magnetic fields B_0 in Eq. (4) have additional constraints by other parameters in a tokamak because it needs to satisfy the Grad-Shafranov equation[14] for the MHD equilibrium in an axisymmetric geometry

$$\mathrm{R}^2\hat{\nabla}\cdot\left(\frac{1}{\mathrm{R}^2}\hat{\nabla}\Psi\right) + a^2\left(\mu\mathrm{R}^2\frac{dp}{d\Psi} + \frac{1}{2}\frac{dF^2}{d\Psi}\right) = 0, \tag{9}$$

where $\nabla\Psi = \mathrm{B}_p\mathrm{R}$, $F = \mathrm{B}_t\mathrm{R}$, and $p = nT$. The background magnetic fields $\mathrm{B}_0 = \sqrt{\mathrm{B}_t^2 + \mathrm{B}_p^2}$ are determined by both toroidal magnetic fields B_t and poloidal magnetic fields B_p. This equation implies the balance between three terms by $\mathrm{B}_p^2/2\mu$, $\mathrm{B}_t^2/2\mu$, and p, and so, the similarity of the equation can be described by two dimensionless parameters $\beta_0 = 2\mu p/\mathrm{B}_0^2$ and $q = (a/\mathrm{R})(\mathrm{B}_t/\mathrm{B}_p)$.

It is coincidental that the scaling in Sec. II B for Maxwell's equations is consistent with the Grad-Shafranov equation. By the scaling in Eqs. (4) and (5), one can prove that β_0 does not change, because $\overline{\beta_0} = \alpha^2\gamma^2\beta_0 = \beta_0$. The ratio of toroidal and poloidal magnetic fields is also conserved by the Grad-Shafranov equation, giving the same safety factor with the same aspect ratio a/R in the scaling, $\bar{q} = q$.

As a result of the scaling, the MHD equilibria have the scalings of pressure and magnetic fields

$$\bar{p} = \alpha^2 p, \quad \overline{\mathrm{B}_t} = \alpha \mathrm{B}_t, \quad \overline{\mathrm{B}_p} = \alpha \mathrm{B}_p, \tag{10}$$

and the plasma current does not change

$$\bar{\mathrm{I}} = \mathrm{I}, \tag{11}$$

where $\mu_0 I = \int dl B_p \propto B_p R$ is used.

C. Fokker-Planck equation

For a moderate or large power RF system, the wave propagation and damping are significantly affected by the plasma distribution function in velocity space. The evolution of the distribution function f is obtained by solving the Fokker-Planck equation

$$\frac{\partial f}{\partial t} + \mathbf{v}\cdot\nabla f + \mathbf{a}\cdot\nabla_v f = C(f), \tag{12}$$

where $C(f)$ is the Fokker-Planck collision operator and $\mathbf{a}$ is the acceleration by the electromagnetic force. In the drift-kinetic equation for a tokamak, the Fokker-Planck equation can be reduced to

$$\frac{\partial f}{\partial t} + (\mathbf{v}_\mathbf{D} + v_{\|}\mathbf{b})\cdot\nabla f + \nabla_v\cdot\mathbf{D}\cdot\nabla_v f = C(f), \tag{13}$$

where $\mathbf{v}_\mathrm{D} = -(v_\perp^2/2\mathrm{B}\omega_c)\mathbf{b}\times\nabla\mathrm{B} - (v_{\|}^2/\omega_c)\mathbf{b}\times(\mathbf{b}\cdot\nabla\mathbf{b})$ is the ∇B and the curvature drift, $v_\perp$ and $v_{\|}$ are the perpendicular and parallel velocities, and $\mathbf{D}$ is the quasilinear velocity diffusion tensor by RF waves.[13,26] The quasilinear diffusion by the RF waves is sufficiently valid if the perturbation due to the waves is small enough to be linearized.[27–29] The quasilinear diffusion tensor was analytically derived by Kennel and Engelmann,[26] and it has been used in many numerical codes (e.g., AORSA-CQL3D[23] and TORIC-CQL3D[30,31]). The term related to the drift $\mathbf{v}_\mathrm{D}$ is small except for the energetic ions, and so, it can be ignorable in this study for RF waves.[15] Taking the bounce average of Eq. (13), the parallel streaming term related to $v_{\|}\mathbf{b}$ is eliminated,[15] giving

$$\frac{\partial f}{\partial t} + \nabla_v\cdot\langle\mathbf{D}\rangle_b\cdot\nabla_v f = \langle C(f)\rangle_b, \tag{14}$$

where the distribution is described by the invariant variables (e.g., energy and magnetic moment) at each flux surface and $\langle\ldots\rangle_b$ is the bounce average. The effect of ignoring the drift term (e.g., finite orbit width effect) to the similarity will be discussed in Sec. V.

As a result of the scaling in Eq. (5), the thermal velocity does not change, $\overline{v_t} = v_t$. Thus, the scaling of the quasilinear term is determined by the RF diffusion tensor $\mathbf{D}$. Using the Kennel-Engelmann diffusion tensor[26]

$$\mathbf{D} \sim \left(\frac{q\mathbf{E}}{m}\right)^2\delta(\omega - \Omega - k_{\|}v_{\|}), \tag{15}$$

the scalings of Eqs. (3) and (7) result in

$$\bar{\hat{\mathbf{D}}}(\bar{\omega}, \overline{B_0}, \bar{n}, \bar{R}, \bar{T}) = \alpha \hat{\mathbf{D}}(\omega, B_0, n, R, T), \tag{16}$$

where δ is the Dirac-delta function and $\hat{\mathbf{D}} = \mathbf{D}/P_{abs}$ is the normalized quasilinear tensor by the power absorption. Equation (16) is obtained by the scaling of the Dirac-delta function in the velocity space using $\delta(\omega - \Omega - k_\parallel v_\parallel) \sim 1/k_\parallel \sim R$.

The collision operator is proportional to the collision frequency, $\nu \propto n/v^3$, and the scaling results in

$$\bar{C}(f) = \alpha^2 C(f). \tag{17}$$

To match the scalability between the RF wave diffusion term and the collision term, we need an additional scaling condition for the RF power

$$\overline{P_{abs}} = \alpha P_{abs}, \tag{18}$$

and then the bounce-averaged Fokker-Planck equation in Eq. (14) is consistent with the scaling of Maxwell's equation and the Grad-Shafranov equation.

Then, the final scaling that we found in this section can be summarized by

$$\begin{aligned} &\bar{\omega} = \alpha\omega, \quad \bar{R} = \frac{1}{\alpha}R, \quad \bar{T} = T, \\ &\overline{B_0} = \alpha B_0, \quad \bar{n} = \alpha^2 n \ \overline{P_{abs}} = \alpha P_{abs}, \end{aligned} \tag{19}$$

where only one scaling parameter α is used. In Eq. (A6), three scaling parameters are used when the plasma mass and species are flexible.

III. NUMERICAL VERIFICATION OF THE SCALING

In this section, we verify the numerical codes, which are widely used in the RF wave research community, using the similarity relation of Eq. (19) derived in Sec. II. The coupling between Maxwell's equations and the Grad-Shafranov equation is tested using the wave code TORIC[20] and the MHD equilibrium code ECOM.[21] As a default case of the test, the ICRF minority heating scenario of (H)D plasmas is examined for a circular plasma shape, which is similar to Alcator-C geometry.[22] The default case has the following parameters: $\omega = 118$ MHz, $R = 64$ cm, $T = 1.65$ KeV, $B_0 = 8$ T, and $n = 2.75 \times 10^{20}$ m^{-3}, and in the scaling cases, the parameters are scaled by α using Eq. (19). The density ratio of Hydrogen to electron ($n_H/n_e = 0.06$) does not change in the scalings. Figure 1 shows the numerical error of the similarity for the normalized electric fields in Eq. (7) for the change by α compared to the default case of $\alpha = 1$. The errors are obtained by measuring the infinite norm of the electric field component (E_+) real part on the 2-D grid of TORIC and its relative ratio of the difference between the scaling case and the default case to the default case. Figure 1(a) shows the relative error of the solutions coupling Maxwell's equation solver in TORIC with the MHD equilibrium built in TORIC.[20] The error is negligibly small within seven significant digits, and it is mostly due to a round-off error. It is worth noting that the round-off error in Fig. 1(a) generally increases when comparing two systems in a big difference of $log_{10}\alpha$, and the degree of the error is almost symmetric in $\alpha = 1$ (i.e., the error between $\alpha = 1$ and $\alpha = 10$ is similar to the error between $\alpha = 1$ and $\alpha = 0.1$). On the other hand, in Fig. 1(b), the result using the numerical coupling between two separate codes TORIC-ECOM shows some loss of accuracy because of the errors in the interpolation on the different radial and poloidal grids between two codes. The ECOM code numerically generates the circular MHD equilibrium in the EFIT format with the corresponding pressure and toroidal magnetic field profiles to the different α, and it is read by TORIC through the conversion of the EFIT format to the numerical equilibrium format of TORIC. Nevertheless, the accuracy in Fig. 1(b) is still acceptable in many practical applications for the RF wave modeling.

To include the kinetic effects due to the non-Maxwellian distribution, the numerical solutions for Maxwell's equations, the Grad-Shafranov equation, and the Fokker-Planck equation

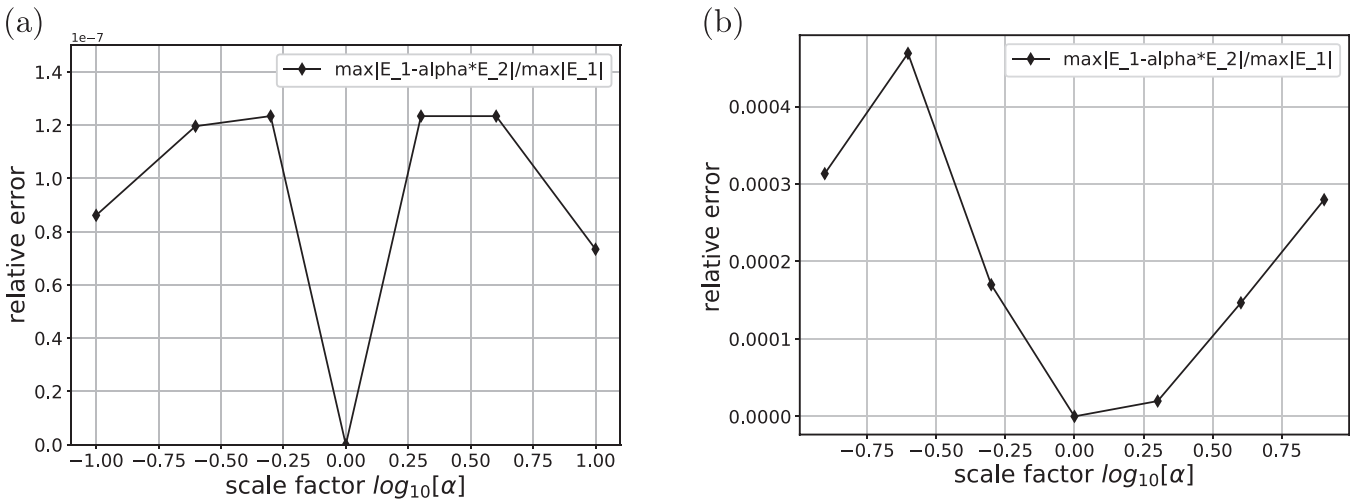

FIG. 1. Relative errors in the similarity of $\hat{\mathbf{E}}$ in Eq. (7) in terms of the scaling parameter α, compared to $\hat{\mathbf{E}}$ of $\alpha = 1$. The solutions are obtained by coupled Maxwell's equation solver and the Grad-Shafranov equation solver using (1) TORIC-analytical circular MHD equilibrium[20] and (b) TORIC-numerical MHD equilibrium code ECOM.[21]

are coupled in the codes, AORSA-ECOM-CQL3D. In Figs. 2 and 3, the similarity of the coupled solutions is verified. Because the bounce-averaged Fokker-Planck equation in Eq. (14) results in the distribution function,

$$f(E,\mu,t) = f(t=0) + \int_{t\prime=0}^{t\prime=t} dt' \left(\langle C(f) \rangle_b - \nabla_v \cdot \langle \mathbf{Q} \rangle_b \cdot \nabla_v f \right), \quad (20)$$

the similarity in Eq. (19) results in the scaling of the size of the distribution function and the time scale of the temporal change

$$\bar{\hat{f}}\left(\bar{\omega}, \overline{B_0}, \bar{R}, \bar{n}, \bar{T}, \overline{P_{abs}}; \bar{t}\right) = \hat{f}(\omega, B_0, R, n, T, P_{abs}; t), \quad (21)$$

$$\bar{t} = \frac{1}{\alpha^2} t, \quad (22)$$

where $\hat{f} = f/n$ is the normalized distribution function by the density.

Figure 2 shows the similarity of 1-d radial power damping profiles between $\alpha = 1$ (solid lines) and $\alpha = 0.1$ (dashed lines) using the solutions of the coupled codes, AORSA-ECOM-CQL3D, through two examples [ICRF off-axis damping in Fig. 2(a) and on-axis damping in Fig. 2(b)]. The on-axis damping case uses the same default parameters as the case of the minority damping in Fig. 1, while the off-axis damping case uses the different wave frequency $\omega = 115$. For the kinetic effects, the total wave power is set to be $P_{abs} = 1$ MW in the default case. The power profiles using the Maxwellian distribution function are obtained in the coupling of two codes, AORSA-ECOM, without coupling with CQL3D. The power profiles using the self-consistent non-Maxwellian distribution are obtained in the coupling of the three codes, after AORSA is iterated with CQL3D, and both solutions converge within several steps in the simple fixed-point iteration.[23] In the self-consistent solution, the difference of power profiles between AORSA and CQL3D is sufficiently small and the relative change over the iteration step is less than 10^{-3}.[23] In Fig. 2, the numerical errors of the scaling between $\alpha = 1$ (solid lines) and $\alpha = 0.1$ (dashed line) are acceptably small within a few percents except the core damping $r/a \sim 0.0$ in Fig. 2(b). The error is likely due to the different treatment of the flux surface at the core in AORSA and CQL3D, and the small difference in the core results in the notable difference in the power density because of the small volume. It is also worth noting that the errors become larger when using non-Maxwellian distribution, which implies that the coupling between AORSA and CQL3D results in the error.

Figure 3 shows the similarity of the distribution functions between $\alpha = 1$ (solid lines) and $\alpha = 0.1$ (dashed line) in the same example of Fig. 2(a). The acceptably small errors in Figs. 3(a) and 3(b) confirm the scalings of the distribution function in Eqs. (21) and (22), respectively.

IV. CONSISTENCY WITH TRANSPORT SCALING

In this section, the consistency of the scaling in Eq. (19) with the particle and energy transport equations is considered. This consistency is a critical question when demonstrating the similarity in real experiments. While the wave frequency, power, and the machine size may be controllable as in the similarity, the plasma density and temperature are not easily controlled because they depend on the particle and energy transport, which are not still clearly understood in the research community. In the transport equation, one needs to consider the sources of energy (e.g., RF wave power damping) and particle (e.g., neutron beam injection) and the sinks of them due to the anomalous transport in a tokamak.[1–3]

For the consistency analysis, we focus on the energy transport rather than the particle transport because one can use fueling to control the density profile and it is not related to the RF waves (except the small nonlinear effects such as the ponderomotive forces[32]). We also assume that the only energy source is

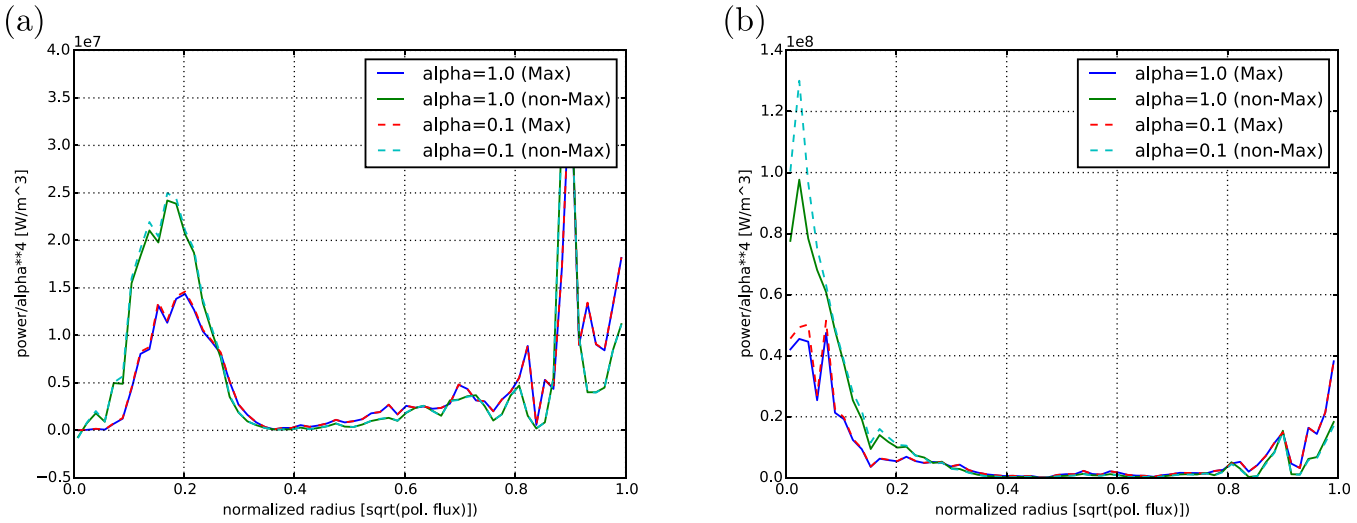

FIG. 2. Power density radial profiles with $\alpha = 1.0$ (solid lines) and $\alpha = 0.1$ (dashed lines) by the solutions of the coupled Maxwell/Grad-Shafranov/Fokker-Planck equations using AORSA-ECOM-CQL3D for (a) 115 MHz ICRF off-axis damping and (b) 118 MHz ICRF on-axis damping.

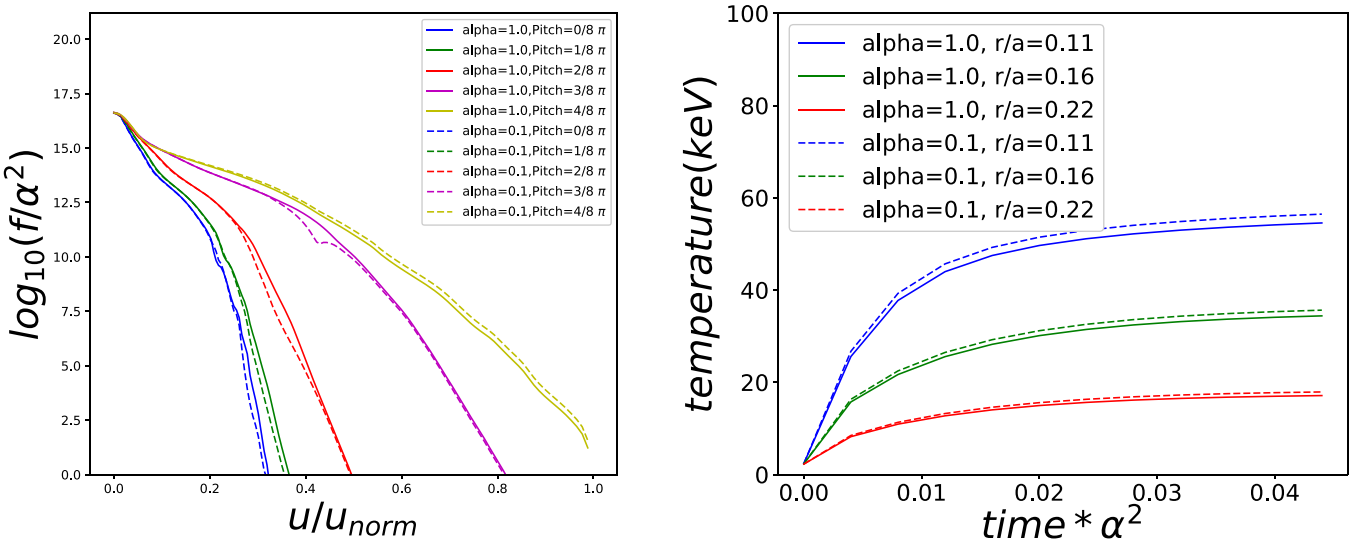

FIG. 3. Comparison of coupled Maxwell's equations/Grad-Shafranov equation/Fokker-Planck equation using AORSA-ECOM-CQL3D for 115 MHz ICRF off-axis damping between $\alpha = 1.0$ (solid lines) and $\alpha = 0.1$ (dashed lines): (a) The distribution function f in the normalized momentum for various pitch angles at $r/a = 0.14$ and (b) the energy of minority species in time for various normalized minor radii r/a.

the RF wave injection (without the neutron beam and ohmic heatings) for simplicity. A simple energy balance equation using the pressure is

$$\frac{d(3nT)}{dt} = P_{RF} - \frac{3nT}{\tau_e}, \tag{23}$$

where P_{RF} is the power density of the RF wave energy transfer and τ_e is the plasma confinement time. In a steady state, the balance between two terms on the right hand side of Eq. (23) determines the temperature profiles by the given density profile. Using the scaling of P_{abs} in Eq. (19) and $P_{RF} \propto P_{abs}/R^3$, the power density has the scaling $\overline{P_{RF}} = \alpha^4 P_{RF}$.

Due to the complicated characteristics of micro/macro-turbulence in a tokamak, there is no complete formula for the confinement time τ_e. In the next three subsections, the consistency is investigated using three different types of estimation for τ_e which have been obtained experimentally or theoretically.

A. Goldston empirical scaling

One of the simple confinement scalings is Goldston scaling[2] that is obtained empirically in a simple form

$$\tau_e = \frac{I^2}{nT} f_1\left(\frac{R}{a}, \frac{b}{a}\right), \tag{24}$$

where f_1 is a geometric factor in terms of the aspect ratio R/a and the elongation parameter b/a. In the scaling of this paper, the plasma current as well as the geometric shape does not change by Eq. (11). Thus, the scaling of the confinement time is determined by $\tau_e \propto 1/nT$, and Eq. (23) in a stead state results in

$$(\bar{n}\bar{T})^2 \propto \overline{P_{RF}}, \tag{25}$$

which is consistent with the scalings in Eq. (19). Thus, the transport by the Goldston scaling for the confinement is consistent with the scalings for the RF waves in Sec. II.

B. Gyro-Bohm scaling

It has been found that the energy transport in the modern tokamak is likely determined by micro-turbulence, which is experimentally measured and theoretically estimated to follow the Gyro-Bohm scale transport.[3,24,25] The diffusion by the Gyro-Bohm scale can be described by

$$D_{GB} = c_s \rho_s \rho^\star f_2(\nu^\star, \beta, q), \tag{26}$$

where f_2 can be a complicated function in terms of dimensionless parameters for collisionality $\nu^\star$, β, and q.[24,25] Here, the dimensionless parameters are defined by

$$\begin{aligned} \rho^\star &= \rho/a, \\ \nu^\star &= (R/r)^{3/2} q R \nu_e / v_{te}^{1/2}. \end{aligned} \tag{27}$$

Because $\rho^\star \propto 1/aB$ and $\nu^\star \propto Rn$, the scaling in Eq. (19) results in $\bar{\beta} = \beta$, $\overline{\rho^\star} = \rho^\star$, and $\overline{\nu^\star} = \alpha\nu^\star$.

If one ignores the weak dependency of collisionality $\nu^\star$ in f_2[3] for simplicity, the scaling results in

$$\begin{aligned} \overline{D_{GB}} &= \alpha^{-1} D_{GB}, \\ \overline{\tau_e} &= \alpha^{-1} \tau_e, \end{aligned} \tag{28}$$

where $\tau_e = a^2/D$ is used. By the scalings $\bar{n} = \alpha^2 n$ and $\overline{P_{RF}} = \alpha^4 P_{RF}$ in Eq. (19), Eqs. (23) and (28) result in

$$\bar{T} = \alpha T, \tag{29}$$

which is not consistent with the scaling for the temperature in Eq. (19). The transport by the Gyro-Bohm scaling results in the increase in the temperature by α.

C. Empirical scaling for ITER design

Using the empirical fitting formula for the confinement time based on many experimental results of the ELMy H-mode, which is used for ITER design[3]

$$\tau_e = 0.0503 H_H I^{0.91} B^{0.15} n^{0.44} P_{abs}^{-0.65} R^{2.05} \kappa^{0.72} M^{0.13} \left(\frac{a}{R}\right)^{0.57}, \quad (30)$$

the scaling of τ_e according to Eq. (19) is

$$\overline{\tau_e} = \alpha^{0.15+2\times0.44-0.65-2.05} \tau_e = \alpha^{-1.67} \tau_e. \quad (31)$$

As a result of Eqs. (23) and (31), the temperature changes by

$$\bar{T} = \alpha^{0.33} T, \quad (32)$$

which is also inconsistent with the scaling for the temperature in Eq. (19). However, the degree of the temperature scaling by α is much smaller than that of the Gyro-Bohm parameter in Eq. (29), and so, the scaling of Eq. (32) may be acceptably consistent with the scaling in Eq. (19), if α is sufficiently close to 1 (e.g., $0.5 < \alpha < 2$ results in $0.75 < \alpha^{0.33} < 1.26$).

V. DISCUSSION

This paper investigates the scaling relations of many parameters of the RF wave system in a tokamak, which satisfy three types of equations (Maxwell's equations, Grad-Shafranov equation, and Fokker-Planck equation) and their consistency with the transport scalings. One can suggest a test system (wind tunnel) similar to the original RF system using the scaling relations in Eq. (19). For example, the existing parameters for ICRF ^3He minority damping in ITER are shown in the left column of Table I, while the scaled parameters by $\alpha = 2$ are shown in the right column of the table. The test system by $\alpha = 2$ can have the reduced size, which is similar to the size of the JET tokamak,[10] and so, building the test system may cost much less than ITER. However, there are several practical problems in building the test system, which increase the cost significantly. First, the background magnetic fields need to increase by twofold, which are about three times larger than JET. Second, the plasma current needs to be the same as ITER, which is about four times larger than JET. The RF frequency and power, which are twice as large as ITER, also increase the cost significantly. Physically, even if one assumes that the plasma density that is four times larger is achievable, obtaining the same temperature as ITER is still questionable, as shown in Secs. IV B and IV C.

TABLE I. A possible test system for the ITER ICRF system.

	ITER ICRF	$\alpha = 2$ test system
Wave frequency	50 MHz	100 MHz
Major radius	6.2 m	3.1 m
Magnetic fields	5.3 T	10.6 T
Plasma current	18.7 MA	18.7 MA
Density	1.0×10^{20} m^{-3}	4.0×10^{20} m^{-3}
Temperature	25 KeV	25 KeV
RF power	20 MW	40 MW

The scaling relations in Eq. (19) are not valid, if the magnetic drift of particles is not negligible in the Fokker-Planck equation for RF waves. In this case, the second and third terms on the left hand side in Eq. (13) are comparable, and the second term has the scaling relation

$$\overline{(\mathbf{v_D} + v_{\parallel \mathbf{b}}) \cdot \nabla} = \alpha (\mathbf{v_D} + v_{\parallel \mathbf{b}}) \cdot \nabla, \quad (33)$$

which is different from that of the collision term in the equation.

The perturbed particle orbit due to RF waves can result in a scaling of the RF wave power that is different from Eq. (18). As the wave energy density becomes larger, the perturbed orbit effect becomes more important and the quasilinear wave diffusion may become problematic. In this case, the nonlinear diffusion in the phase space needs to be considered, and the radial particle diffusion also becomes more important.[33,34]

The similarity of this study may conclude that there are many physical and engineering possibilities to invalidate the practical test system for the RF wave system in a tokamak. Nevertheless, there are two types of lessons learned from this study. First, for the same wave physics, the scaling of the machine size is in the opposite direction to the scalings of magnetic fields and wave frequency and power. These inverse relations are likely to prohibit the cost reductions for the test system. Particularly, the increase in the RF total power for the reduced size system is non-intuitive, but it is necessary for the same kinetic effects due to non-Maxwellian distribution because of the increased plasma density and collisionality. Second, the coupled codes (e.g., TORIC-ECOM and AORSA-ECOM-CQL3D) are verified to satisfy the similarity relations within the allowable range of errors. It is also useful to evaluate the accuracy of the coupling between the codes and diagnose a possible numerical problem. For example, it is found that the numerical error of the coupling in a certain radius range [e.g., $r/a < 0.1$ in Fig. 2(b)] is notably larger than other radii, which means that some calculations are treated differently between the codes at the particular radius.

ACKNOWLEDGMENTS

The author would like to thank Dr. Lee Berry and Ms. Suh Yoon Kang for the insightful and helpful advice on this study and paper. This work was supported by the research fund of Hanyang University (HY-2018), U.S. DoE Contract No. DE-FC02-01ER54648 under a Scientific Discovery through Advanced Computing Initiative. This research used resources of MIT and NERSC by U.S. DoE Contract No. DE-AC02-05CH11231.

APPENDIX: SCALING FOR THE SPECIES MASS AND CHARGE FLEXIBILITY

The scaling relations in Eq. (19) can be different when the plasma mass and charge are adjustable. One may imagine the situations, in which electron mass and charge are flexible or the contribution of electrons to the wave propagation and

damping is negligibly small. Then, the species mass and charge in the scaling can be modified by selecting ion species of different mass and charge.

Then, the four scaling parameters can be used: the wave frequency by a multiplication factor α, the mass by β, the major radius by γ, and the charge by ζ

$$\bar{\omega} = \alpha\omega, \quad \bar{m} = \beta m, \quad \bar{\mathrm{R}} = \gamma \mathrm{R}, \quad \bar{\mathrm{Z}} = \zeta \mathrm{Z}, \tag{A1}$$

where the overline of the variable denotes the change in the variable after the scaling.

For the same dimensionless variables in the dielectric tensor by the scalings in Eq. (A1), it needs to satisfy

$$\overline{\mathrm{B}_0} = \alpha\beta\zeta^{-1}\mathrm{B}_0, \quad \bar{n} = \alpha^2\beta\zeta^{-2}n, \quad \bar{\mathrm{T}} = \beta \mathrm{T}, \tag{A2}$$

where Eq. (5) is used.

The scalings of Eqs. (A1) and (7) result in

$$\bar{\hat{\mathbf{D}}}\left(\bar{\omega}, \overline{\mathrm{B}_0}, \bar{n}, \bar{\mathrm{R}}, \bar{m}, \bar{\mathrm{Z}}, \bar{\mathrm{T}}\right) = \frac{\zeta^2}{\beta^2}\alpha\hat{\mathbf{D}}(\omega, \mathrm{B}_0, n, \mathrm{R}, m, \mathrm{Z}, \mathrm{T}). \tag{A3}$$

Because the collision frequency, $\nu \propto nZ^2/m^2v^3$, depends on the mass, the collision operator scaling follows

$$\bar{\mathrm{C}}(f) = \frac{\alpha^2}{\beta}\mathrm{C}(f). \tag{A4}$$

To match the scalability between the RF wave diffusion term and the collision term, the RF power needs to have the scalability

$$\overline{P_{abs}} = \frac{\alpha\beta}{\zeta^2}P_{abs}. \tag{A5}$$

The scalings for the flexible mass and charge can be summarized by

$$\begin{aligned} &\bar{\omega} = \alpha\omega, \quad \bar{\mathrm{R}} = \frac{1}{\alpha}\mathrm{R}, \quad \bar{m} = \beta m, \quad \bar{\mathrm{T}} = \beta \mathrm{T}, \quad \bar{\mathrm{Z}} = \zeta \mathrm{Z}, \\ &\overline{\mathrm{B}_0} = \alpha\beta\zeta^{-1}\mathrm{B}_0, \quad \bar{n} = \alpha^2\beta\zeta^{-2}n, \quad \overline{P_{abs}} = \frac{\alpha\beta}{\zeta^2}P_{abs}. \end{aligned} \tag{A6}$$

REFERENCES

[1]J. W. Connor and J. B. Taylor, Nucl. Fusion **17**, 1047 (1977).
[2]R. J. Goldston, Plasma Phys. Controlled Fusion **26**, 87 (1984).
[3]ITER Physics Expert Groups on Confinement and Transport, ITER Physics Expert Group on Confinement Modeling and Database, and ITER Physics Basis Editors, Nucl. Fusion **39**, 2175 (1999).
[4]L. Mydlarski and Z. Warhaft, J. Fluid Mech. **320**, 331 (1996).
[5]D. Ryutov, R. P. Drake, J. Kane, E. Liang, B. A. Remington, and W. M. Wood-Vasey, Astrophys. J. **518**, 821 (1999).
[6]W.-T. Lin and C.-L. Ho, Ann. Phys. **327**, 386 (2012).
[7]ITER Physics Expert Group on Energetic Particles, Heating and Current Drive, and ITER Physics Basis Editors, Nucl. Fusion **39**, 2495 (1999).
[8]P. U. Lamalle, M. J. Mantsinen, J.-M. Noterdaeme, B. Alper, P. Beaumont, L. Bertalot, T. Blackman, V. V. Bobkov, G. Bonheure, J. Brzozowski, C. Castaldo, S. Conroy, M. de Baar, E. de la Luna, P. de Vries, F. Durodie, G. Ericsson, L.-G. Eriksson, C. Gowers, R. Felton, J. Heikkinen, T. Hellsten, V. Kiptily, K. Lawson, M. Laxåback, E. Lerche, P. Lomas, A. Lyssoivan, M.-L. Mayoral, F. Meo, M. Mironov, I. Monakhov, I. Nunes, G. Piazza, S. Popovichev, A. Salmi, M. I. K. Santala, S. Sharapov, T. Tala, M. Tardocchi, D. Van Eester, B. Weyssow, and JET EFDA Contributors, Nucl. Fusion **46**, 391–400 (2006).
[9]M.-L. Mayoral, P. U. Lamalle, D. Van Eester, E. A. Lerche, P. Beaumont, E. De La Luna, P. De Vries, C. Gowers, R. Felton, J. Harling, V. Kiptily, K. Lawson, M. Laxåback, P. Lomas, M. J. Mantsinen, F. Meo, J.-M. Noterdaeme, I. Nunes, G. Piazza, M. Santala, and JET EFDA Contributors, Nucl. Fusion **46**, S550 (2006).
[10]P. U. Lamalle, A. M. Messiaen, P. Dumortier, and F. Louche, Nucl. Fusion **46**, 432–443 (2006).
[11]A. Messiaen, P. Dumortier, V. Kyrytsya, F. Louche, and M. Vervier, Fusion Eng. Des. **86**, 855 (2011).
[12]F. Durodiéa, M. Nightingaleb, A. Argouarchc, G. Berger-Byc, T. Blackmanb, J. Caughmand, V. Cocilovoe, P. Dumortiera, P. Edwardsb, J. Fanthomeb, D. Frigionee, R. Gouldingd, M. Grahamb, J. Hobrikf, S. Huygena, S. Jachmicha, P. Jacquetb, A. Kayeb, P. U. Lamalleg, E. Lerchea, T. Loarerc, M.-L. Mayoralb, A. Messiaena, I. Monakhovb, M. F. F. Naveh, K. Nichollsb, J. Ongenaa, F. Riminic, D. Van Eestera, M. Verviera, M. Vranckena, C. Sozzie, D. Storkb, M. Tsalasi, A. Waldenb, A. Whitehurstb, K.-D. Zastrowb, JET EDFA Contributors JET EFDA, and Culham Science Centre, Fusion Eng. Des. **84**, 279 (2009).
[13]T. H. Stix, *Waves in Plasmas* (AIP Press, 1992).
[14]H. Grad and H. Rubin, J. Nucl. Energy **7**, 284 (1958).
[15]R. W. Harvey and M. G. McCoy, in *Proceedings of the IAEA Technical Committee Meeting on Advances in Simulation and Modeling of Thermonuclear Plasmas*, Montreal (1992), p. 489.
[16]Y. V. Petrov and R. W. Harvey, Plasma Phys. Controlled Fusion **58**, 115001 (2016).
[17]M. Brambilla and R. Bilato, Nucl. Fusion **49**, 085004 (2009).
[18]A. Devred, I. Backbier, D. Bessette, G. Bevillard, M. Gardner, C. Jong, F. Lillaz, N. Mitchell, G. Romano, and A. Vostner, Supercond. Sci. Technol. **27**, 044001 (2014).
[19]B. N. Sorbom, J. Ball, T. R. Palmer, F. J. Mangiarotti, J. M. Sierchio, P. Bonoli, C. Kasten, D. A. Sutherland, H. S. Barnard, C. B. Haakonsen, J. Goh, C. Sung, and D. G. Whyte, Fusion Eng. Des. **100**, 378 (2015).
[20]M. Brambilla, Plasma Phys. Controlled Fusion **41**, 1 (1999).
[21]J. P. Lee and A. Cerfon, Comput. Phys. Commun. **190**, 72 (2015).
[22]T. D. Shepard, C. L. Fiore, F. S. McDermott, R. R. Parker, and M. Porkolab, AIP Conf. Proc. **159**, 262 (1987).
[23]E. F. Jaeger, R. W. Harvey, L. A. Berry, J. R. Myra, R. J. Dumont, C. K. Phillips, D. N. Smithe, R. F. Barrett, D. B. Batchelor, P. T. Bonoli, M. D. Carter, E. F. D'azevedo, D. A. D'ippolito, R. D. Moore, and J. C. Wright, Nucl. Fusion **46**, S397 (2006).
[24]R. E. Waltz, J. C. DeBoo, and M. N. Rosenbluth, Phys. Rev. Lett. **65**, 2390 (1990).
[25]F. W. Perkins, C. W. Barnes, D. W. Johnson, S. D. Scott, M. C. Zarnstorff, M. G. Bell, R. E. Bell, C. E. Bush, B. Grek, K. W. Hill, D. K. Mansfield, H. Park, A. T. Ramsey, J. Schivell, B. C. Stratton, and E. Synakowski, Phys. Fluids B **5**, 477 (1993).
[26]C. F. Kennel and F. Engelmann, Phys. Fluids **9**, 2377–2388 (1966).
[27]J. R. Cary, D. F. Escande, and A. D. Verga, Phys. Rev. Lett. **65**, 3132 (1990).
[28]G. Laval and D. Pesme, Plasma Phys. Controlled Fusion **41**, A239 (1999).
[29]J. P. Lee, P. T. Bonoli, and J. C. Wright, Phys. Plasmas **18**, 012503 (2011).
[30]J. P. Lee, J. C. Wright, N. Bertelli, E. F. Jaeger, E. Valeo, R. W. Harvey, and P. T. Bonoli, Phys. Plasmas **24**, 052502 (2017).
[31]N. Bertelli, E. J. Valeo, D. L. Green, M. Gorelenkova, C. K. Phillips, M. Podestà, J. P. Lee, J. C. Wright, and E. F. Jaeger, Nucl. Fusion **57**, 056035 (2017).
[32]J. R. Myra and D. A. D'Ippolito, Phys. Plasmas **9**, 3867 (2002).
[33]L. G. Eriksson and P. Helander, Phys. Plasmas **1**, 308–314 (1994).
[34]T. Johnson, T. Hellsten, and L.-G. Eriksson, Nucl. Fusion **46**, S433 (2006).